Science and Technology Indonesia
e-ISSN:2580-4391 *p*-ISSN:2580-4405
Vol. 8, No. 4, October 2023

Research Paper

Monitoring the Muara Laboh Geothermal Field in Indonesia using the ISBAS Method with Sentinel-1 SAR Images

Mokhamad Yusup Nur Khakim[1]*, Takeshi Tsuji[2], Erni[1], Akhmad Aminudin Bama[1], Frinsyah Virgo[1], Muhammad Irfan[1], Azhar Kholiq Affandi[1], Toshifumi Matsuoka[3]

[1]*Department of Physics, Faculty of Mathematics and Natural Sciences, Sriwijaya University, Indralaya, 30862, Indonesia*
[2]*School of Engineering, University of Tokyo, 7-3-1 Hongo, Bunkyo-ku, Tokyo, 113-8654, Japan*
[3]*Fukada Geological Institute, Hon-Komagome 2-13-12, Bunkyo-ku, Tokyo, 113-0021, Japan*
***Corresponding author**: myusup_nkh@mipa.unsri.ac.id

Abstract
The Muara Laboh geothermal field lies in a South Solok basin zone, West Sumatra, Indonesia. Production and reinjection of geothermal fluids into the underground reservoir commonly induce crustal deformation. The study area is covered by 63.8% plantation, primary, and secondary forests, which limit the ability of conventional InSAR techniques. Therefore, an Intermittent Small BASeline Subset (ISBAS) analysis has been performed to estimate line-of-sight (LOS) displacement time series due to geothermal production using the Sentinel-1 dataset between 8 March 2021 and 15 March 2022. The localized subsidence with ~30 mm/yr rate over this tropical geothermal field has been revealed by using the ISBAS. The subsidence coincides with an area of the Muara Laboh geothermal reservoir. We suggest that geothermal production induced subsidence. In addition, the deformation in this geothermal field was controlled by faults and seasonally influenced by rainfall. Therefore, deformation variation was correlated with fluctuations in rainfall patterns. The geothermal reservoir system exhibited elastic expansion in response to seasonal recharge events during the rainy season.

Keywords
Geothermal, Deformation, Synthetic Aperture Radar, ISBAS Method, Sentinel-1

Received: 30 May 2023, Accepted: 11 August 2023
https://doi.org/10.26554/sti.2023.8.4.626-631

1. INTRODUCTION

Sumatra Island is tectonically related to the oblique sinking of the Indo-Australian Plate under the Eurasian Plate. It has an important role in creating the Great Sumatra Fault (GSF), a series of volcanic activities, and geothermal systems. This GSF system, segmented with compression and extension zones, is northwest-southeast dextral strike-slip faults along the Sumatra island (~1,900 km) from Banda Aceh in the northwest to Bandar Lampung in the southeast (Mussofan et al., 2018). The fault system determines the island's geothermal activity structurally.

The Muara Laboh geothermal field lies in a depression zone between the Siulak and Suliti fault segments located in the south and north, respectively. This geothermal field is in the South Solok Regency, West Sumatra, Indonesia (Figure 1). The geothermal power plant in this field has officially operated with a capacity of 80 MWe since last December 2019 (Hutter, 2020). Production and reinjection of geothermal fluids into the underground reservoir commonly induce crustal deformation. The reservoir's in-situ stress field significantly affects the combined hydraulic and deformation mechanisms (Soltanzadeh et al., 2009). Detectable and monitored deformation can provide essential insights into reservoir extent and dynamics.

Synthetic aperture radar interferometry (InSAR) techniques can be applied to observe the ground surface deformation, which can estimate the deformation of the host rock caused by fluid migration at depth. Small surface deformations with an accuracy of 1 cm or less and sizeable spatial area coverage (up to several tens of square kilometers) can be imaged at any time of day or night, regardless of the weather, with the InSAR techniques (Khakim et al., 2013). Differential InSAR (DInSAR) is the first radar interferometry technique to measure deformation (Gabriel et al., 1989). Measured deformation from the InSAR technique was successfully used to infer the sources' depths, locations, shapes, and relative deformation magnitudes over Eastern California's Coso geothermal site (Fialko and Simons, 2000). Previous studies of the DInSAR technique were

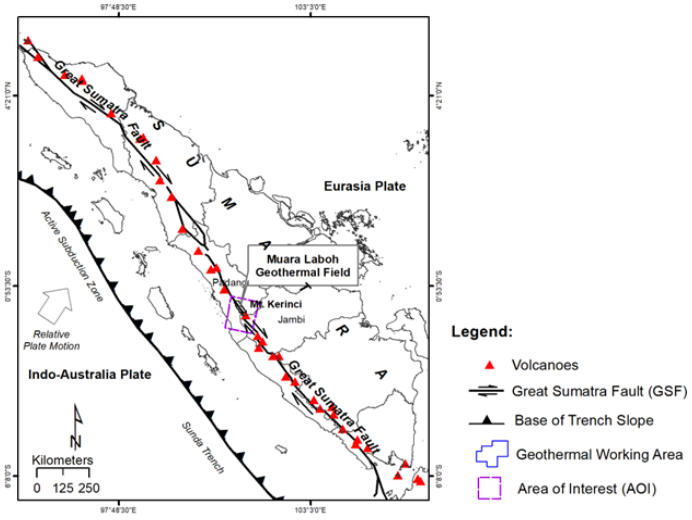

Figure 1. Location of the Study Area

also applied in other geothermal fields, such as the Mexicali Valley, Baja California, Mexico (Sarychikhina et al., 2010) and Mexico's Cerro Prieto geothermal field (Sarychikhina et al., 2016).

However, the DInSAR is problematic when the phase difference of reflected radar waves from a ground element cannot be interpreted as deformation, such as vegetation change and variation in atmospheric conditions. This limitation can be overcome by developing multi-temporal InSAR approaches, such as Persistent Scatterer Interferometry (PSI) (Crosetto et al., 2010) and Small BASeline Subset (SBAS) (Berardino et al., 2002; Khakim et al., 2023; Lanari et al., 2015). These conventional PSI and SBAS are effective methods for measuring surface deformations in typically urbanized regions or bare rock outcrops. Furthermore, an intermittent SBAS (ISBAS) method is a modified implementation of the SBAS approach providing a better image of the spatial extent of the land deformation (Sowter et al., 2013). The ISBAS method was mostly applied in environment studies, such as urban subsidence (Liu et al., 2020), coal mining (Bateson et al., 2015; Novellino et al., 2014; Sowter et al., 2013), and peatland monitoring (Alshammari et al., 2020; Alshammari et al., 2018; Marshall et al., 2018), but still limited in the geothermal study. This ISBAS was used in the Tengiz oil field (Grebby et al., 2019) and has not been applied in a tropical geothermal field. The Tengiz oil field is in a region that has a semi-arid climate. However, our study area is one of the tropical geothermal fields, mostly covered by forest with tall trees and dense vegetation. In addition, there is no deformation measurement for the current state in this field.

Therefore, this study aims to estimate spatiotemporal deformation over the tropical Muara Laboh geothermal field and surrounding area by modifying the ISBAS method and using the Sentinel-1 image. The estimated deformation is important for geodynamic monitoring and characterization during geothermal energy production.

2. EXPERIMENTAL SECTION

2.1 Materials

This study utilized the European Space Agency's (ESA) Sentinel-1 IW TOPS images. The Sentinel-1 uses a C-band Synthetic Aperture Radar (SAR) sensor with a central frequency of 5.405 GHz and a wavelength of 5.6 cm to offer continuous worldwide all-weather, day-and-night radar imagery. The benefits of this dataset over competing offerings include a larger coverage area, a shorter revisit period (12 days), and no cost to the user. Therefore, a higher spatial and temporal resolution of surface deformation monitoring is possible with a time-series analysis based on this data (Yalvac, 2020). We used 32 descending Sentinel-1A Single Look Complex (SLC) images with a path of 3 and a frame of 617 from 8 March 2021 to 15 March 2022.

2.2 Methods

ISBAS-DInSAR Analysis. A processing flow of spatiotemporal deformation is presented in Figure 2. We used open-source GMTSAR software for InSAR data processing on the Ubuntu 18.04 platform (Sandwell et al., 2011). Twenty-two descending SLC images were used to generate 111 interferometric pairs. The SLC image of 19 September 2021 was used as a super-master image selected automatically using the Sentinel Application Platform (SNAP) software version 7.0.

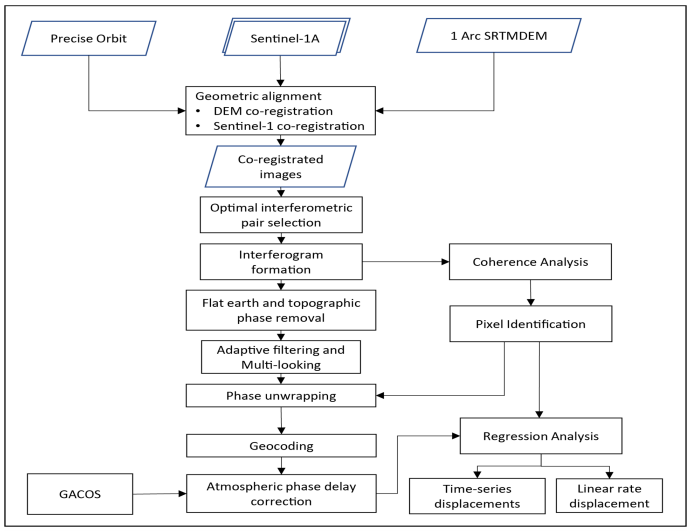

Figure 2. The Processing Flow of Spatiotemporal Deformation

The other SLCs, as slave images, are geometrically aligned with the super-master image (Shirzaei et al., 2017; Xu et al., 2020). The alignment of slave scenes to a super-master scene started with a pixel-wise estimation of range and azimuth offsets using precise orbits and the 1-arcsecond shuttle radar topography mission (SRTM) digital elevation model (DEM), which covers the area of the SLC images (Xu et al., 2017). This

process was done to align the SLC images with the master image properly. The spatial and temporal baseline thresholds to form interferometric pairs are 50 m and 100 days, respectively. These perpendicular and temporal baseline networks are presented in Figure 3.

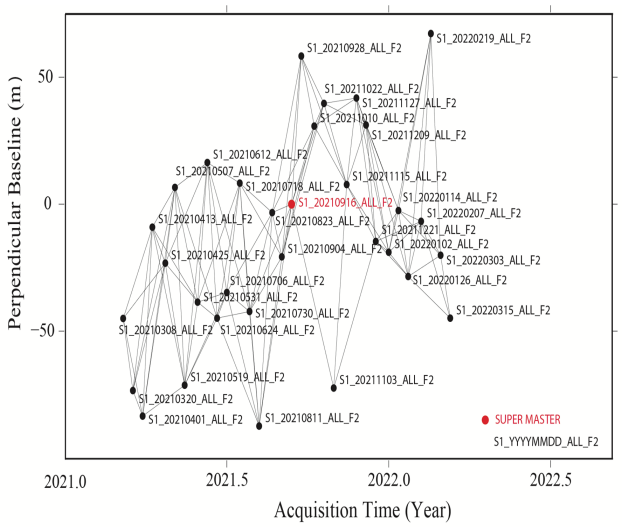

Figure 3. Perpendicular and Temporal Baseline Networks to Derive Interferometric Pairs from 8 March 2021 to 15 March 2022; A Red Dot Denotes a Super-Master Image

Using the SRTM DEM, the topographic phase was subtracted from the measured interferometric phase. In addition, a Gaussian filter with a half-width of 200 m was used to eliminate the phase term from the speckle noises, and it was multi-looking by factors of 8 pixels in range and 2 pixels in azimuth. Phase interferograms were unwrapped by applying a SNAPHU algorithm (Chen and Zebker, 2001) and a coherence threshold 0.2. The interferometric phase images were successfully unwrapped and then projected onto a map coordinate system WGS84. Then, the atmospheric phase delay was removed from the original interferogram using the Generic Atmospheric Correction Online Service (GACOS) (Yu et al., 2018) (Figure 4). After the atmospheric correction, we applied a best-fit plane to eliminate the interferograms' remaining linear trends.

The study area is covered by 63.8% plantation, primary, and secondary forests (Figure 5). Therefore, spatiotemporal deformation is derived by modifying the ISBAS algorithm. Our modified ISBAS has applied a convolution filter type of boxcar with a width of 0.7s. The deformation estimation was performed only on coherence points. The coherence threshold of 0.20 was applied to the generated interferogram for the ISBAS analysis. A minimum quality criterion is applied to select enough quality in a minimum number of interferograms to be accepted for analysis.

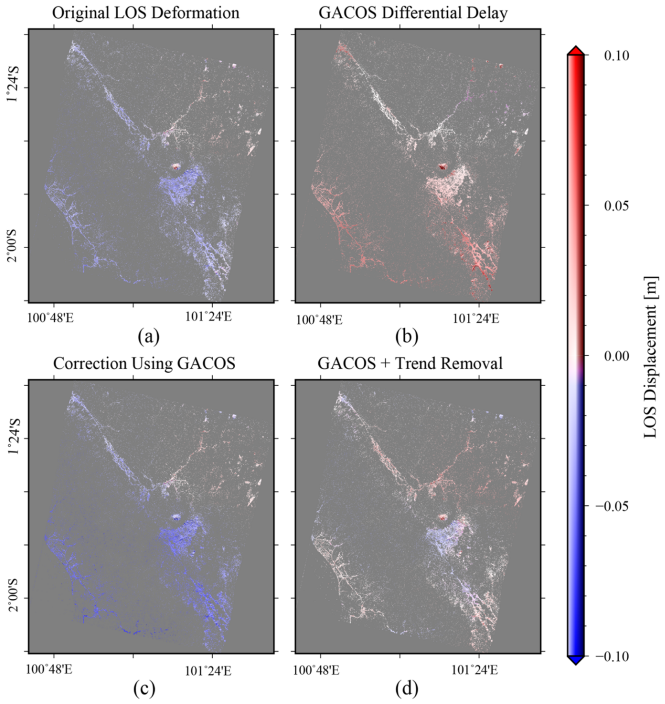

Figure 4. Atmospheric Correction and Residual Linear Trend Removal

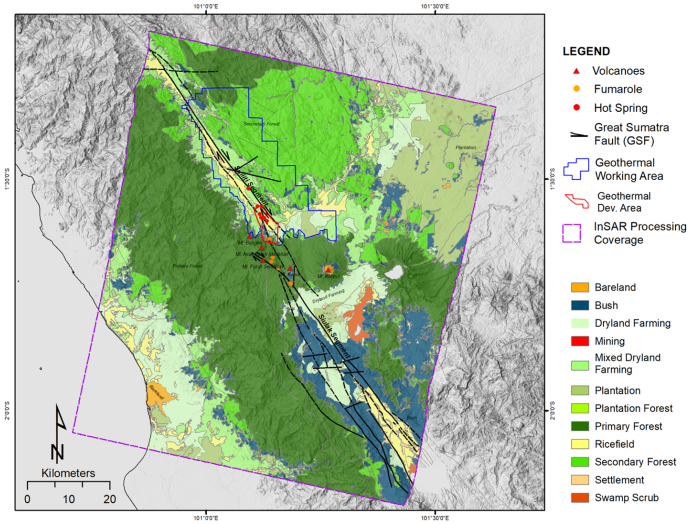

Figure 5. Landcover of the Study Area

3. RESULTS AND DISCUSSION

3.1 Surface Deformation Rate

The working area of Muara Laboh geothermal lies within the Suliti Fault Segment of the Great Sumatra Fault (GSF), as presented as a blue polygon area in the left panel of Figure 6. The positive deformation values in this figure indicate motion towards the satellite, which can be interpreted as surface uplift. In contrast, negative values indicate motion away or surface

subsidence. The offset of right dilatation along the segment is an area that is the center of the volcanic activity. This fault section accommodates a geothermal heat-producing magmatic intrusion (Mussofan et al., 2018). This Suliti Fault Segment structure has high permeability for Muara Laboh geothermal system and provides multiple conduits for magma moving up (Alamsyah, 2012). Consequently, the uplift around the Suliti Fault segment occurred with the rate reaching about 15 mm/yr, proving that the area along this fault segment is the potential for a geothermal system.

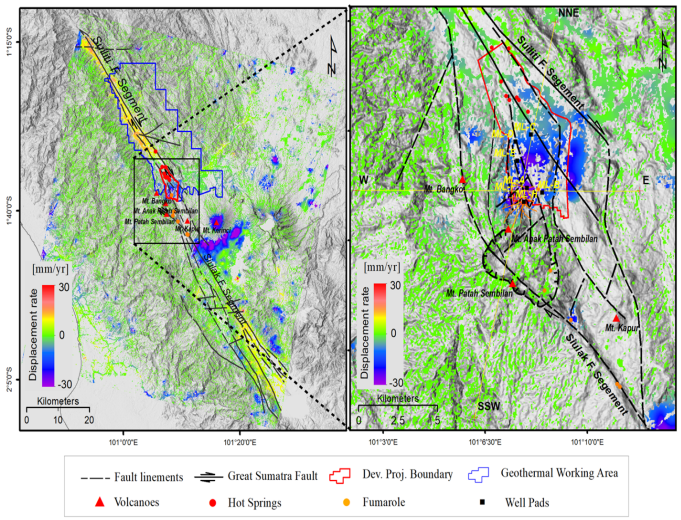

Figure 6. Subsidence Rate of Muara Laboh Geothermal Field

The right panel of Figure 6 clearly shows the Muara Laboh geothermal field exhibiting noticeable surface subsidence. The subsidence around well pads was patterned irregularly. The observed deformation is interpreted as dominantly resulting from geothermal fluid production, so the subsidence patterns appear to follow the distribution of production wells. A linear subsidence rate in the LOS direction reached approximately 30 mm/yr over this geothermal field between March 2021 and March 2022. The geological structure of this site might cause an irregular pattern of subsidence. This area is a junction between two main segments, i.e., the Suliti Fault segment and the Siulak Fault segment, creating several faults between these two segments. These inferred faults might control the subsidence.

Consequently, the pattern of the subsidence in the southwest Muara Laboh field indicates a reservoir segmented by these faults. Moreover, the reservoir might undergo compaction due to overburden and pressure loss from the reservoir during fluid production. The reactivation of subsurface geological features due to production may threaten the structural stability of the reservoir seal and cause fluids to migrate to adjacent formations naturally. In addition, production levels in a formation may drop due to subsidence-caused compaction that reduces porosity.

3.2 Time Series and Profiles of Deformation

The subsidence profiles are compared to the geological condition of the geothermal field. Larger magnitudes of ground surface subsidence occurred near areas where production wells exist, such as the ML-A and ML-H wells (Figure 7). Fluid geothermal extraction from the shallower reservoir induced the subsidence. However, the deformation around the injection well, ML-B, appears to form an anticline shape of the profiles. The pressure of fluid injection into the deeper reservoir causes an uplift. Moreover, a geothermal manifestation, such as Idung Mancung fumarole, indicates fluid flow from underground to the surface. The pressure might further contribute to the surface deformation profile's anticline shape.

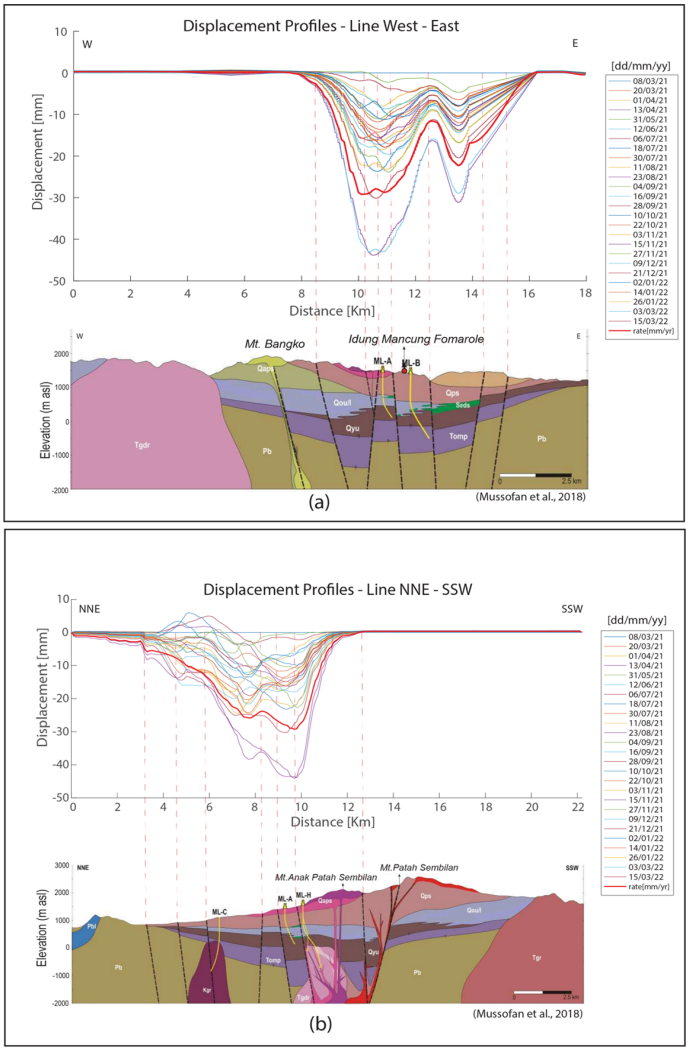

Figure 7. Profiles of Displacement Time Series Marked W-E and NNE-SSW in Figure 6 with the Geology Cross-Sections

Furthermore, ground surface displacements varied at seven well pads with rainfall between March 2021 and March 2022 (Figure 8). Generally, the displacements were correlated with rainfall variation. In addition, the displacement trends tended

to decrease in common due to geothermal fluid production. Subsidence with larger magnitudes, as expected, occurred around production wells of ML-A, ML-F, and ML-H. Meanwhile, the area associated with ML-B, ML-D, and ML-E injection wells should have trends of cumulative deformation in the form of anticline profiles. As they are close to production wells, the ground surface at their sites subsides by several millimeters, following the subsidence pattern at production wells. Their subsidence magnitudes were expected to be lower than those at production wells.

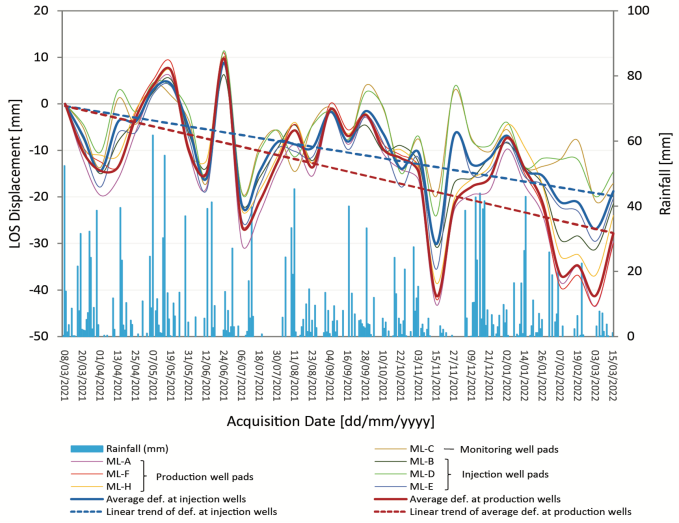

Figure 8. Displacement Time Series Variation with Rainfall at the Seven Well Pads

4. CONCLUSION

This report discusses geodetic data observed at a Muara Laboh geothermal potential junction zone between the Suliti and Siulak Fault segments. The ISBAS method has successfully revealed surface deformation at this geothermal field. The maximum subsidence rate of ~30 mm/yr is interpreted as resulting dominantly from geothermal fluid production, so the subsidence patterns appear to follow the distribution of production wells.

Faults might control the subsidence, which can be identified near the well pad cluster in the east part of the field. Moreover, the identified surface uplift rate was about 15 mm/yr due to the activity of the suiliti and siulak fault segments in the west and east of the study area, respectively. Fluid movement from deep inside the earth to the surface, manifested as the Idung Mancung fumarole, is suggested to contribute to surface deformation. In addition to fluid production/injection and faults, rainfall influenced the variation of the deformation.

The findings have implications not only for the geothermal exploitation that is still going on but also for the potential risk to development. Measuring this type of deformation improves our understanding of the complexity of the spatial extent and dynamics of the geothermal field, which may be essential for the resource's exploitation.

5. ACKNOWLEDGMENT

We would like to acknowledge Universitas Sriwijaya for financial support through "Penelitian Hibah Kompetitif", Contract Number: 0118.93/UN9/SB3.LP2M.PT/2022, dated 17 Mei 2022. We also thank the European Space Agency (ESA) for providing Sentinel-1 data, anonymous reviewers, and the academic editor for their valuable comments and suggestions.

REFERENCES

Alamsyah, O. (2012). Sitting Reinjection Well Pad under Exploration Phase, Liki Pinagawan Muaralaboh Case. In *Proceedings of the 1st ITB Geotherma Workshop*

Alshammari, L., D. S. Boyd, A. Sowter, C. Marshall, R. Andersen, P. Gilbert, S. Marsh, and D. J. Large (2020). Use of Surface Motion Characteristics Determined by InSAR to Assess Peatland Condition. *Journal of Geophysical Research: Biogeosciences*, **125**(1); e2018JG004953

Alshammari, L., D. J. Large, D. S. Boyd, A. Sowter, R. Anderson, R. Andersen, and S. Marsh (2018). Long-Term Peatland Condition Assessment Via Surface Motion Monitoring using the ISBAS DInSAR Technique Over the Flow Country, Scotland. *Remote Sensing*, **10**(7); 1103

Bateson, L., F. Cigna, D. Boon, and A. Sowter (2015). The Application of the Intermittent SBAS (ISBAS) InSAR Method to the South Wales Coalfield, UK. *International Journal of Applied Earth Observation and Geoinformation*, **34**; 249–257

Berardino, P., G. Fornaro, R. Lanari, and E. Sansosti (2002). A New Algorithm for Surface Deformation Monitoring based on Small Baseline Differential SAR Interferograms. *IEEE Transactions on Geoscience and Remote Sensing*, **40**(11); 2375–2383

Chen, C. W. and H. A. Zebker (2001). Two-dimensional Phase Unwrapping with Use of Statistical Models for Cost Functions in Nonlinear Optimization. *Journal of the Optical Society of America. A*, **18**(2); 338–351

Crosetto, M., O. Monserrat, R. Iglesias, and B. Crippa (2010). Persistent Scatterer Interferometry. *Photogrammetric Engineering & Remote Sensing*, **76**(9); 1061–1069

Fialko, Y. and M. Simons (2000). Deformation and Seismicity in the Coso Geothermal Area, Inyo County, California: Observations and Modeling using Satellite Radar Interferometry. *Journal of Geophysical Research: Solid Earth*, **105**(B9); 21781–21793

Gabriel, A. K., R. M. Goldstein, and H. A. Zebker (1989). Mapping Small Elevation Changes Over Large Areas: Differential Radar Interferometry. *Journal of Geophysical Research: Solid Earth*, **94**(B7); 9183–9191

Grebby, S., E. Orynbassarova, A. Sowter, D. Gee, and A. Athab (2019). Delineating Ground Deformation Over the Tengiz Oil Field, Kazakhstan, using the Intermittent SBAS (ISBAS)

DInSAR Algorithm. *International Journal of Applied Earth Observation and Geoinformation*, **81**; 37–46

Hutter, G. (2020). Geothermal Power Generation in the World 2015–2020 Update Report. In *Proceedings of the World Geothermal Congress, Reykjavik, Iceland*, volume 26

Khakim, M. Y. N., S. Supardi, and T. Tsuji (2023). Earthquake Affects Subsidence in Jakarta using Sentinel-1A Time Series Images and 2D-MSBAS Method. *Vietnam Journal of Earth Sciences*, **45**(1); 111–130

Khakim, M. Y. N., T. Tsuji, and T. Matsuoka (2013). Detection of Localized Surface Uplift by Differential SAR Interferometry at the Hangingstone Oil Sand Field, Alberta, Canada. *IEEE Journal of Selected Topics in Applied Earth Observations and Remote Sensing*, **6**(6); 2344–2354

Lanari, R., P. Berardino, M. Bonano, F. Casu, C. De Luca, S. Elefante, A. Fusco, M. Manunta, M. Manzo, C. Ojha, et al. (2015). Sentinel-1 Results: SBAS-DInSAR Processing Chain Developments and Land Subsidence Analysis. In *2015 IEEE International Geoscience and Remote Sensing Symposium (IGARSS)*. IEEE, pages 2836–2839

Liu, L., J. Yu, B. Chen, and Y. Wang (2020). Urban Subsidence Monitoring by SBAS-InSAR Technique with Multi-Platform SAR Images: A Case Study of Beijing Plain, China. *European Journal of Remote Sensing*, **53**(sup1); 141–153

Marshall, C., D. J. Large, A. Athab, S. L. Evers, A. Sowter, S. Marsh, and S. Sjögersten (2018). Monitoring Tropical Peat Related Settlement using ISBAS InSAR, Kuala Lumpur International Airport (KLIA). *Engineering Geology*, **244**; 57–65

Mussofan, W., M. C. Baroek, J. Stimac, R. P. Sidik, I. Ramadhan, and S. Santana (2018). Geothermal Resource Exploration Along Great Sumatera Fault Segments in Muara Laboh: Perspectives from Geology and Structural Play. In *Proceedings, 43rd Workshop on Geothermal Reservoir Engineering*. Stanford University Stanford, CA

Novellino, A., A. D. Athab, M. A. bin Che Amat, M. F. Syafiudin, A. Sowter, S. Marsh, F. Cigna, and L. Bateson (2014). Intermittent SBAS Ground Motion Analysis in Low Seismicity Areas: Case Studies in the Lancashire and Staffordshire Coalfields, UK. *Seismology from Space: Geodetic Observations and Early Warning of Earthquakes. Royal Astronomical Society, Burlington House, Piccadilly, London, UK*; 8–9

Sandwell, D., R. Mellors, X. Tong, M. Wei, and P. Wessel (2011). GMTSAR: An InSAR Processing System based on Generic Mapping Tools. *Scripps Institution of Oceanography Technical Report*; 1–31

Sarychikhina, O., E. Glowacka, and J. Mojarro (2016). Surface Deformation Associated with Geothermal Fluids Extraction at the Cerro Prieto Geothermal Field, Baja California, Mexico Revealed by DInSAR Technique. *Living Planet Symposium*, **740**; 294

Sarychikhina, O., E. Glowacka, F. Suarez-Vidal, and R. Mellors (2010). DInSAR Analysis of Land Subsidence Caused by Geothermal Fluid Exploitation in the Mexicali Valley, BC, Mexico. *IAHS-AISH Publ*, **339**; 268–273

Shirzaei, M., R. Bürgmann, and E. J. Fielding (2017). Applicability of Sentinel-1 Terrain Observation by Progressive Scans Multitemporal Interferometry for Monitoring Slow Ground Motions in the San Francisco Bay Area. *Geophysical Research Letters*, **44**(6); 2733–2742

Soltanzadeh, H., C. Hawkes, P. McLellan, and S. Smith (2009). Poroelastic Modelling of Production and Injection-Induced Stress Changes in a Pinnacle Reef. *Proceedings of RockEng09, Rock Engineering in Difficult Conditions*, **7016**; 1–12

Sowter, A., L. Bateson, P. Strange, K. Ambrose, and M. F. Syafiudin (2013). DInSAR Estimation of Land Motion using Intermittent Coherence with Application to the South Derbyshire and Leicestershire Coalfields. *Remote Sensing Letters*, **4**(10); 979–987

Xu, X., D. T. Sandwell, and B. Smith-Konter (2020). Coseismic Displacements and Surface Fractures from Sentinel-1 InSAR: 2019 Ridgecrest Earthquakes. *Seismological Research Letters*, **91**(4); 1979–1985

Xu, X., D. T. Sandwell, E. Tymofyeyeva, A. Gonzalez-Ortega, and X. Tong (2017). Tectonic and Anthropogenic Deformation at the Cerro Prieto Geothermal Step-Over Revealed by Sentinel-1A InSAR. *IEEE Transactions on Geoscience and Remote Sensing*, **55**(9); 5284–5292

Yalvac, S. (2020). Validating InSAR-SBAS Results by Means of Different GNSS Analysis Techniques in Medium-and High-Grade Deformation Areas. *Environmental Monitoring and Assessment*, **192**(2); 120

Yu, C., Z. Li, N. T. Penna, and P. Crippa (2018). Generic Atmospheric Correction Model for Interferometric Synthetic Aperture Radar Observations. *Journal of Geophysical Research: Solid Earth*, **123**(10); 9202–9222

